Heat and Mass Transfer in a Channel with Surface Mass Addition: Application to Phase Change Processes

E. M. SPARROW and H. S. YU

University of Minnesota, Minneapolis, Minnesota

The heat and mass transfer processes in a binary mixture flowing in a parallel plate channel with mass addition at the bounding surfaces are investigated analytically. The rate of mass addition, the temperature, and the mass fraction are arbitrarily prescribed at each of the bounding walls. Similarity solutions are evaluated numerically to yield pressure gradient, Nusselt number, and Sherwood number results for a wide range of each of three governing parameters. It is found that increasingly strong surface mass addition markedly increases the magnitude of the axial pressure gradient. Mass addition decreases the Nusselt and Sherwood numbers at the channel wall at which the injection is strongest but may actually increase these moduli at the opposite wall. A generalizing analysis is performed to accommodate phase change processes as well as to accommodate the specification of plenum conditions rather than wall surface conditions. Application is made to the evaporation of liquid water by an air stream. It is shown that the rate of evaporation is augmented as the rate of air injection increases, but the extent of the augmentation is less than the causative increase in the air flow rate.

This paper is concerned with heat and mass transfer processes for laminar flow in a parallel plate channel. The research is subdivided into two distinct phases, the first of which generates fundamental results which are subsequently applied in the second. In the first phase, consideration is given to the situation wherein there are prescribed rates of mass transfer into the channel from the bounding surfaces, the respective rates at each surface being independently and arbitrarily prescribable. The temperatures of the bounding walls and the concentrations of the components of a binary mixture are also arbitrarily prescribed and are maintained at different values for each wall. For these conditions, Nusselt number and Sherwood number results are determined for a wide range of values of three independent parameters, which include the Prandtl or Schmidt numbers, the ratio of the injection rates at the walls, and the injection Reynolds number.

The aforementioned results may be applied to various physical situations, both directly and through generalizing analysis. In the second portion of this investigation, such a generalizing analysis is performed to accommodate: surface mass transfer resulting from a change of phase; surface temperatures, concentrations, and mass transfer rates which are determined by equilibrium requirements instead of being specified a priori; and specification of thermal and concentration conditions in the supply chamber of the injected fluid rather than at the surface of the duct wall. In performing the generalizing analysis, consideration is given to the situation wherein one wall of the channel is covered with an evaporable (or sublimable) material while a gas, unsaturated in the evaporable vapor, is injected into the channel at the other wall. To illustrate the application of the generalized analysis, evaporation rates and surface temperatures are calculated for the case of evaporation of water into an injected air stream.

The velocity problem for laminar flow in a parallel plate channel with prescribed suction or injection at the bounding walls was first analyzed by Berman (*1*) for the case of symmetrical surface mass transfer. Additional solutions to Berman's problem have been subsequently contributed by several investigators. More recently, Terrill and Shrestha (*2*) analyzed forced convection channel flow in which the mass transfer rates at each of the bounding walls were assigned different values. Although these authors present an otherwise thoroughgoing treatment of their problem, only sparse information is given for the axial pressure gradient.

Heat transfer in a channel having symmetric surface mass transfer was studied by Terrill (3) for Graetz type of thermal boundary conditions; that is, the walls are at a common, uniform temperature different from the entering fluid temperature. In the near neighborhood of the inlet cross section, the developing thermal boundary layer was analyzed by Gill and co-workers (*4*) by employing the Leveque method. These prior analyses of heat transfer in porous walled channels provide valuable background for the present study but do not contribute directly to the problems under consideration.

PRESCRIBED SURFACE MASS TRANSFER, TEMPERATURE, AND MASS FRACTION

Consideration is first given to the fundamental situation wherein the boundary conditions for heat transfer and mass diffusion are arbitrarily prescribed on the channel walls, and the injection rate at each wall is also arbitrarily prescribed. To facilitate the detailed description of the problem, it is convenient to refer to Figure 1*a*. As shown therein, the channel walls are designated as 1 and 2. Without any loss of generality, let 2 denote the wall having the higher injection rate, so that $|v_2| > |v_1|$. Furthermore, since v is positive in the direction of positive y, it follows that $v_1 > 0$ and $v_2 < 0$ for injection. The injection rates v_1 and v_2 are independent of x and may take on arbitrary magnitudes, the ratio of which is denoted by β, that is

$$\beta = -(v_1/v_2) \tag{1}$$

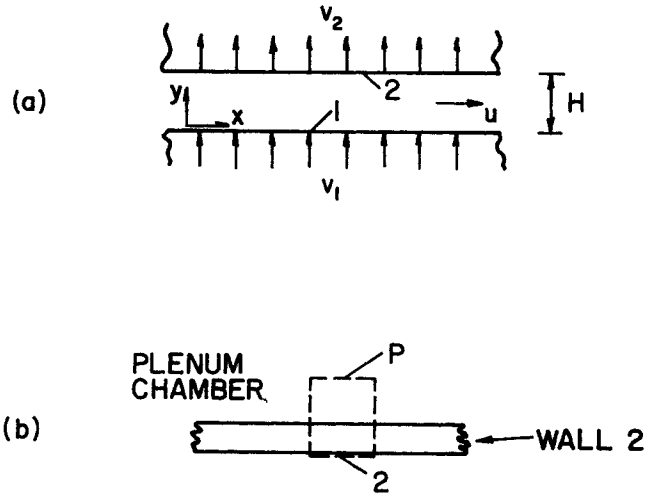

Fig. 1. Schematic of the physical problem.

For mass injection at both surfaces and with $|v_2| > |v_1|$, it follows that

$$0 \leq \beta \leq 1 \tag{1a}$$

One sided injection corresponds to $\beta = 0$, and symmetric injection corresponds to $\beta = 1$.

The temperatures at surfaces 1 and 2 are, respectively, designated as T_1 and T_2. These quantities are stipulated as being independent of x. The fluid emerging from each wall is assumed to be at the surface temperature of that wall.

The flowing fluid may be a binary mixture of gases or of liquids. Let the components of the mixture be designated as i and j and the corresponding local concentrations be specified by the mass fractions* W_i and W_j. From the definition of the mass fraction

$$W_i + W_j = 1 \tag{2}$$

at all points in the channel. Therefore, a knowledge of W_i is tantamount to a knowledge of W_j, and vice versa. The boundary values of W_i will be specified as W_{i1} and W_{i2}, respectively, at walls 1 and 2. These boundary values are independent of x.

With the description of the problem now completed, attention will be turned to its analytical formulation and solution.

Velocity

The first step in the analysis is to formulate the velocity problem. By setting aside the detailed variations of the fluid properties and by using instead a reference state in the evaluation of the final results (Nusselt number, Sherwood number, etc.), the velocity problem is decoupled from the temperature and mass diffusion problems. Thus, the conservation equations appropriate to the velocity problem are

$$\frac{\partial u}{\partial x} + \frac{\partial v}{\partial y} = 0 \tag{3}$$

$$u\frac{\partial u}{\partial x} + v\frac{\partial u}{\partial y} = -\frac{1}{\rho}\frac{\partial p}{\partial x} + \nu\left(\frac{\partial^2 u}{\partial x^2} + \frac{\partial^2 u}{\partial y^2}\right) \tag{4}$$

$$u\frac{\partial v}{\partial x} + v\frac{\partial v}{\partial y} = -\frac{1}{\rho}\frac{\partial p}{\partial y} + \nu\left(\frac{\partial^2 v}{\partial x^2} + \frac{\partial^2 v}{\partial y^2}\right) \tag{5}$$

* Ratio of mass of component to mass of mixture in a given volume.

There exists a similarity solution for Equations (3), (4), and (5). By employing the findings of reference 2, one can write

$$u = \left[\frac{\bar{u}(0)}{1+\beta} - \frac{v_2 x}{H}\right] f'(\eta), \quad v = v_2 f(\eta) \tag{6}$$

in which

$$\eta = \frac{y}{H} \tag{7}$$

and $\bar{u}(0)$ is the mean velocity at the axial station that is designated as $x = 0$. It is readily verified that the continuity Equation (3) is identically satisfied by Equations (6), regardless of f.

Next, after substitution of Equations (6) and (7) into the momentum Equations (4) and (5), one is led to the conclusion that $\partial^2 p/\partial x \partial \eta = 0$, from which it follows that

$$f''' + N_{R_2}(f'^2 - ff'') = \text{const.} \tag{8}$$

or

$$f^{IV} + N_{R_2}(f'f'' - ff''') = 0 \tag{9}$$

where

$$N_{R_2} = v_2 H/\nu \tag{10}$$

The quantity N_{R_2} will be designated as the injection Reynolds number. Since $v_2 < 0$ for injection, so also is $N_{R_2} < 0$.

The boundary conditions on f will now be deduced. The physical conditions that $u(0) = u(H) = 0$, $v(0) = v_1$, and $v(H) = v_2$ become, with the aid of Equations (6)

$$f(0) = -\beta, \quad f'(0) = 0, \quad f(1) = 1, \quad f'(1) = 0 \tag{11}$$

The f function is thus governed by the nonlinear ordinary differential Equation (9) subject to the boundary conditions (11), with N_{R_2} and β as independently prescribable parameters. Direct numerical solutions of this system, although possible, would be tremendously time consuming, even on a very fast computer. This is because, for each N_{R_2}, β pair, one must simultaneously determine the quantities $f''(0)$ and $f'''(0)$ which, taken together with the given $f(0)$ and $f'(0)$, satisfy Equation (9) and the conditions $f(1) = 1$, $f'(1) = 0$. Upon recognizing that on the order of one hundred N_{R_2}, β pairs are necessary to provide sufficiently detailed information in the range of interest, the magnitude of the computational task is readily apparent.

The aforementioned difficulty is somewhat eased by em-

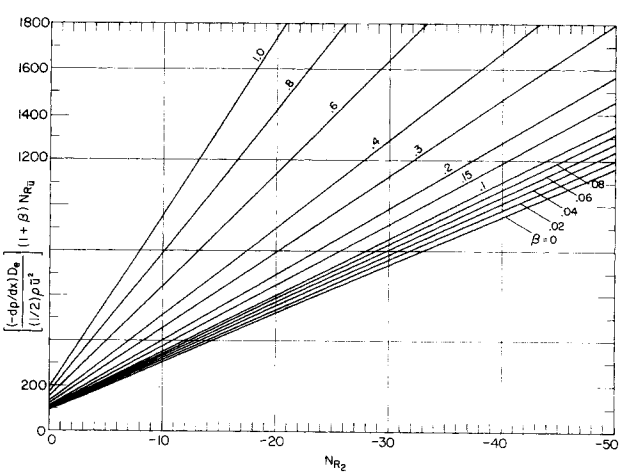

Fig. 2. Axial pressure gradient results.

ploying a change of variables similar to that of Terrill and Shrestha (2)

$$\xi = b\eta, \quad g(\xi) = (N_{R_2}/b)\, f(\eta) \tag{12}$$

so that Equations (9) and (11) become

$$g^{IV} + g'g'' - g''' = 0 \tag{13}$$

$$g(0) = -\beta N_{R_2}/b, \quad g'(0) = 0, \quad g(b) = N_{R_2}/b, \quad g'(b) = 0 \tag{14}$$

Suppose that $g(0)$, $g''(0)$, and $g'''(0)$ are arbitrarily prescribed. These, together with the given $g'(0) = 0$, are sufficient so that Equation (13) can be forward integrated from $\xi = 0$, say, by the Runge-Kutta method. The integration is continued until the condition $g' = 0$ is encountered. The ξ at which $g' = 0$ is identified as b. Furthermore, the g value corresponding to the $g' = 0$ point is used to find N_{R_2} from the expression $N_{R_2} = bg(b)$. Finally, by making use of the $g(0)$ value assigned at the starting point of the integration, one can calculate $\beta = -bg(0)/N_{R_2}$.

Thus, by employing the foregoing scheme, it is possible to circumvent the laborious task of solving Equations (9) and (11) directly. However, this simplified method also has a drawback, namely, that one cannot prescribe the parameters N_{R_2} and β; rather, N_{R_2} and β emerge as end products. In any final presentation of results (for example, Nusselt number), one of the two quantities N_{R_2} or β will have to appear as a curve parameter. Thus, it is essential that either N_{R_2} or β be restricted to specific values.

It was decided to seek solutions for specific β values in the range between 0 and 1 [see Equation (1a)] for N_{R_2} ranging from 0 to -50, the N_{R_2} emerging as end products of the computational procedure. On the basis of preliminary computational experiments, it was found that $g''(0)$ could be fixed once and for all, provided that the chosen $g''(0)$ was compatible with the large N_{R_2} cases. The thus employed $g''(0)$ was -2.1986. Then, computer runs spanning a wide range of $g(0)$ and $g'''(0)$ were carried out and the narrow ranges containing the desired β and N_{R_2} delineated. Thereafter, runs were made on a trial and error basis until the preselected β values were matched to within twelve significant figures.

By this process, solutions were generated for $\beta = 0$, 0.02, 0.04, 0.06, 0.08, 0.10, 0.15, 0.2, 0.3, 0.4, 0.6, 0.8, and 1.0. The corresponding velocity distributions will be employed in connection with the forthcoming solutions of the energy and diffusion equations. Also, the velocity solutions provide results for the axial pressure gradient, as is now demonstrated.

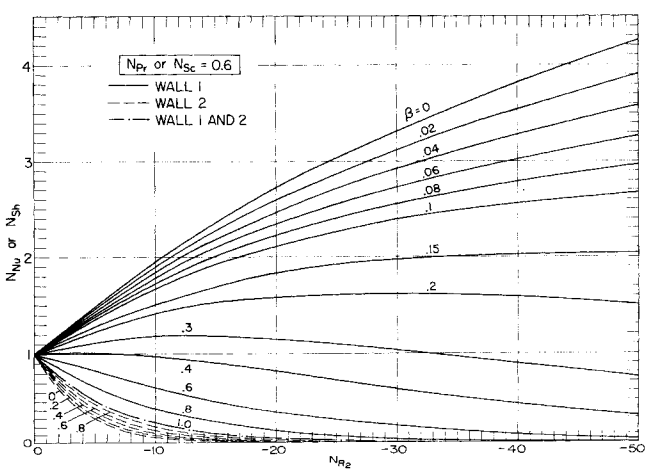

Fig. 3. Nusselt and Sherwood number results, N_{Pr} or $N_{Sc} = 0.6$.

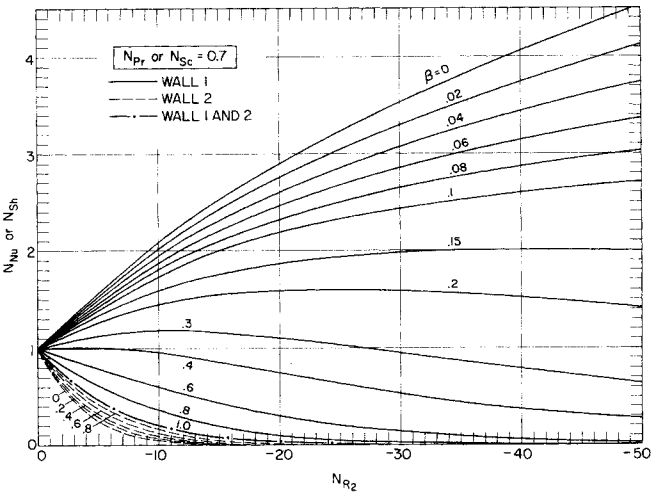

Fig. 4. Nusselt and Sherwood number results, N_{Pr} or $N_{Sc} = 0.7$.

To derive an expression for the axial pressure gradient, one returns to Equation (4) and introduces the transformation (6) and (7), from which there follows after rearrangement

$$\left[\frac{(-dp/dx)D_e}{\frac{1}{2}\rho\bar{u}^2}\right] N_{R_{\bar{u}}} = \frac{8}{1+\beta}\left[N_{R_2}(ff'' - f'^2) - f'''\right] \tag{15}$$

where

$$D_e = 2H, \quad N_{R_{\bar{u}}} = \bar{u}\, D_e/\nu \tag{15a}$$

and

$$\bar{u} = \frac{1}{H}\int_0^H u\,dy = \bar{u}(0) - (1+\beta)(v_2 x/\nu) \tag{15b}$$

In the foregoing, D_e is the equivalent diameter (equal to $2H$), $\bar{u}$ is the mean velocity at any axial station x, and $N_{R_{\bar{u}}}$ is the axial Reynolds number. The bracketed quantity appearing on the left-hand side of Equation (15) may be identified as an apparent fraction factor, including both momentum as well as truly frictional effects. Thus, the product of the apparent friction factor and axial Reynolds number is a function of both N_{R_2} and β. For given values of these parameters, the right-hand side of Equation (15) is independent of the cross-sectional coordinate η. Numerical results for the pressure drop will be presented later.

Heat Transfer and Mass Diffusion

The starting point of the heat transfer analysis is the energy conservation equation

$$u\frac{\partial T}{\partial x} + v\frac{\partial T}{\partial y} = \alpha\left(\frac{\partial^2 T}{\partial x^2} + \frac{\partial^2 T}{\partial y^2}\right) \tag{16}$$

An equation identical in form to (16) describes the conservation of either species i or j. Since global mass conservation, that is, Equation (3), has already been employed, only one of the species conservation equations represents an independent physical condition, and either may be utilized. Thus, for species i

$$u\frac{\partial W_i}{\partial x} + v\frac{\partial W_i}{\partial y} = D\left(\frac{\partial^2 W_i}{\partial x^2} + \frac{\partial^2 W_i}{\partial y^2}\right) \tag{17}$$

For surface temperatures and surface mass fractions that

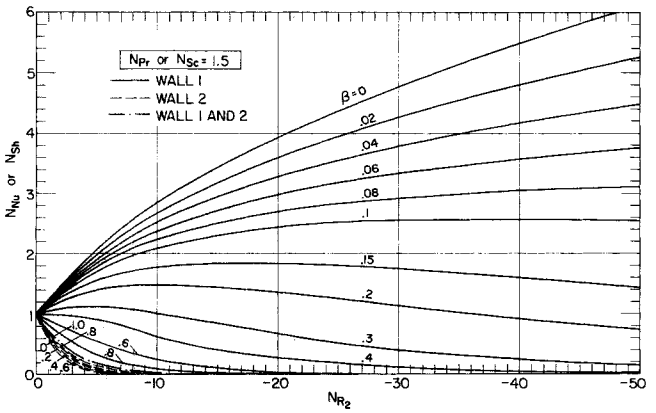

Fig. 5. Nusselt and Sherwood number results, N_{Pr} or $N_{Sc} = 1.5$.

are uniform in x, it is readily demonstrated that $T = T(y)$ and $W_i = W_i(y)$, provided that the flow in the channel is due only to mass injection at the walls. If, on the other hand, there is upstream axial inflow, the distributions $T = T(y)$ and $W_i = W_i(y)$ correspond to the fully developed regime.

By employing the just discussed dependencies for T and W_i, Equations (16) and (17) simplify to

$$v\frac{\partial T}{\partial y} = \alpha\frac{\partial^2 T}{\partial y^2}, \quad v\frac{\partial W_i}{\partial y} = D\frac{\partial^2 W_i}{\partial y^2} \tag{18}$$

Next, by defining dimensionless temperature and mass fraction variables as

$$\Phi_T = \frac{T - T_1}{T_2 - T_1}, \quad \Phi_W = \frac{W_i - W_{i1}}{W_{i2} - W_{i1}} \tag{19}$$

Equations (18) reduce to

$$\Phi'' = N_{R_2}\,\Omega f\Phi' \tag{20}$$

where

$$\Omega_T = \frac{\nu}{\alpha} = N_{Pr}, \quad \Omega_W = \frac{\nu}{D} = N_{Sc} \tag{21}$$

The boundary conditions follow directly from Equation (19), so that

$$\Phi(0) = 0, \quad \Phi(1) = 1 \tag{22}$$

It is evident from the foregoing development that the heat transfer and mass diffusion problems share a common analysis. They also share a common solution, which is

$$\Phi(\eta) = \frac{\int_0^\eta \exp\left[N_{R_2}\,\Omega\int_0^\eta f d\eta\right] d\eta}{\int_0^1 \exp\left[N_{R_2}\,\Omega\int_0^\eta f d\eta\right] d\eta} \tag{23}$$

Since the velocity function f depends parametrically on N_{R_2} and β, it is evident that Φ is parameterized by three quantities: Ω (N_{Pr} or N_{Sc}), N_{R_2} and β. The $\Phi(\eta)$ distributions are evaluated by direct numerical integration of Equation (23) by using the velocity solutions as input.

The heat transfer characteristics may be represented in terms of h and N_{Nu}, which are defined as

$$h_1 = \frac{-k(\partial T/\partial y)_1}{T_1 - T_2}, \quad h_2 = \frac{-k(\partial T/\partial y)_2}{T_1 - T_2},$$

$$N_{Nu_1} = \frac{h_1 H}{k}, \quad N_{Nu_2} = \frac{h_2 H}{k} \tag{24}$$

Similarly, the mass diffusion results may be characterized by employing the mass transfer coefficient K and Sherwood number N_{Sh}:

$$K_1 = \frac{-\rho D(\partial W_i/\partial y)_1}{W_{i1} - W_{i2}}, \quad K_2 = \frac{-\rho D(\partial W_i/\partial y)_2}{W_{i1} - W_{i2}},$$

$$N_{Sh_1} = \frac{K_1 H}{\rho D}, \quad N_{Sh_2} = \frac{K_2 H}{\rho D} \tag{25}$$

Then, upon introducing the solution for Φ given by Equation (23), N_{Nu} and N_{Sh} are expressible as

$$N_{Nu_1} \text{ or } N_{Sh_1} = \left[\int_0^1 \exp\left(N_{R_2}\,\Omega\int_0^\eta f d\eta\right) d\eta\right]^{-1} \tag{26a}$$

$$N_{Nu_2} \text{ or } N_{Sh_2} = \left[\exp\left(N_{R_2}\,\Omega\int_0^1 f d\eta\right)\right] \Big/ \left[\int_0^1 \exp\left(N_{R_2}\,\Omega\int_0^\eta f d\eta\right) d\eta\right] \tag{26b}$$

in which Ω denotes either N_{Pr} or N_{Sc}. Results are extracted from Equations (26a) and (26b) by direct numerical integration.

The Nusselt and Sherwood numbers depend upon parametrically prescribed values of N_{R_2}, β, and Ω. Numerical results will be presented in the next section.

Results

The axial pressure gradient, evaluated from Equation (15), is plotted in Figure 2 as a function of the injection Reynolds number N_{R_2}, with the injection ratio β as curve parameter. The pressure gradient grouping, contained within the brackets, is dimensionless. The factor $(1 + \beta)$, which appears in the ordinate variable, is included to facilitate clarity of presentation. In the absence of this factor, the various curves would lie closer together, making it difficult to distinguish one from another (as in Figure 2 in the neighborhood of $N_{R_2} = 0$). Furthermore, the ordering of the curves with β (that is, ascending order) remains unchanged if the $(1 + \beta)$ factor is omitted from the ordinate.

Inspection of the figure shows that the pressure gradient increases markedly with increasing magnitudes of the injection Reynolds number. This increase in pressure gradient derives mainly from momentum increases resulting from the acceleration of the flow. There is evidence that the high pressure gradients encountered in duct flows with injection tend to postpone the onset of turbulence. For instance, in experiments performed in a circular tube, transition to turbulence was delayed to a Reynolds number as high as

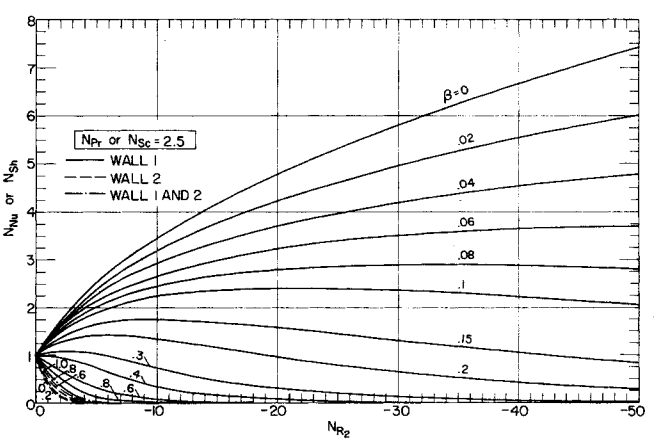

Fig. 6. Nusselt and Sherwood number results, N_{Pr} or $N_{Sc} = 2.5$.

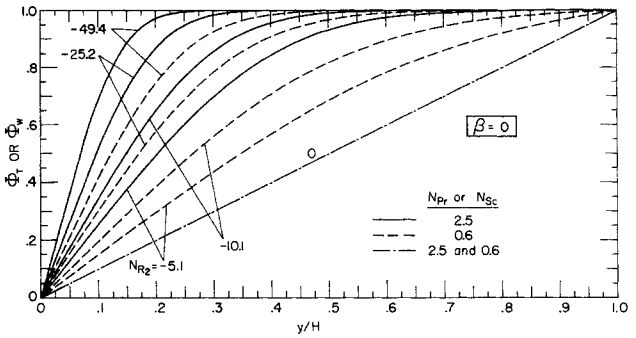

Fig. 7. Representative temperature and mass fraction profiles, $\beta = 0$.

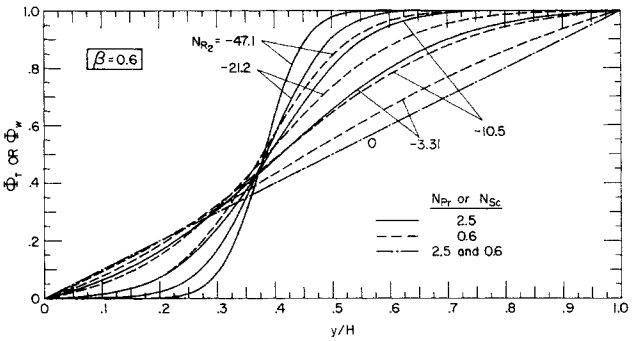

Fig. 8. Representative temperature and mass fraction profiles, $\beta = 0.6$.

10,000 by injection (5). Furthermore, under the action of injection, a low Reynolds number turbulent flow may tend to revert to the laminar regime (6). These findings suggest that laminar flow may have greater practical relevance in the presence of mass injection than when there is no surface mass transfer.

Numerical results for the Nusselt and Sherwood numbers are presented in Figures 3 through 6. The parameter ranges of the Prandtl and Schmidt numbers were chosen with gaseous systems in mind. The Prandtl numbers of most gases lie in the range between 0.6 and 1.0, while Schmidt numbers between 0.6 and 2.5 are characteristic of a wide range of gases and vapors in dilute binary mixture with air (7).

Each of Figures 3 through 6 corresponds to a specific Prandtl or Schmidt number, 0.6, 0.7, 1.5, and 2.5, respectively.* The results are plotted as a function of the injection Reynolds number N_{R_2} for parametric values of the injection ratio β. The curves are drawn as solid or dashed lines, depending upon whether they refer to wall 1 or to wall 2, wherein $|v_2| \geq |v_1|$. When $\beta = 1$, the surface mass transfer is symmetric, that is, $|v_2| = |v_1|$, so that no distinction need be made between the two walls.

Inspection of any one of the figures reveals that walls 1 and 2 respond differently to the presence of surface mass transfer. At wall 2 (the wall with the higher injection rate), mass injection decreases the Nusselt and Sherwood numbers regardless of the value of the injection ratio β. At larger magnitudes of N_{R_2}, N_{Nu_2} and N_{Sh_2} are essentially zero. This behavior results from the blanketing of the wall surface with a layer of fluid whose temperature and mass fraction are essentially equal to those at the wall.

On the other hand, wall 1 shows a variety of responses depending on the value of the injection ratio β. When β is nearly zero, that is $|v_1| << |v_2|$, the effect of injection is to increase the Nusselt and Sherwood numbers, while an opposite effect is in evidence when β is near unity. For intermediate β, N_{Nu_1} and N_{Sh_1} initially increase with increasing $|N_{R_2}|$ and decrease thereafter. These trends are made plausible by noting that conditions in the fluid layer adjacent to wall 1 are affected by two conflicting factors. First, there is the general displacement of the flow toward wall 1 as a result of the relatively stronger mass injection at wall 2; this would tend to increase N_{Nu_1} and N_{Sh_1}. Second, there is the mass injection at wall 1 itself, which would tend to decrease N_{Nu_1} and N_{Sh_1}. The first of these factors predominates when β is very small, while the second factor predominates for larger β.

* Results, similar to those of Figures 3 through 6, were also determined for N_{Pr} or N_{Sc} = 1.0 and 2.0. Owing to space limitations, this information is not presented in the paper but is available from the authors on request.

By making comparisons among Figures 3 through 6, various trends with Prandtl and Schmidt number may be identified. At wall 2, increasing N_{Pr} or N_{Sc} results in a decrease in N_{Nu_2} and N_{Sh_2}. A similar behavior is in evidence at wall 1 at large and moderate β values. Only for very small β values do N_{Nu_1} and N_{Sh_1} increase with increasing Prandtl and Schmidt numbers.

To complement the Nusselt and Sherwood number results, representative temperature and mass fraction profiles are presented in Figures 7 and 8. In each figure, the dimensionless temperature and mass fraction variables, respectively Φ_T and Φ_W, are plotted as a function of the dimensionless cross-sectional coordinate y/H for parametric values of N_{R_2}. Curves are given for the extremes of N_{Pr} or N_{Sc} = 0.6 and 2.5. Figure 7 is for $\beta = 0$, and Figure 8 is for $\beta = 0.6$.

In Figure 7, it is seen that the profile, which is a straight line for $N_{R_2} = 0$, rises more steeply near wall 1 as $|N_{R_2}|$ increases, with a corresponding flattening in the neighborhood of wall 2. These trends are accentuated at higher N_{Pr} or N_{Sc}. A somewhat different behavior is in evidence for $\beta = 0.6$ (Figure 8). In this case, the profiles tend to flatten both in the neighborhood of wall 1 and in the neighborhood of wall 2, with a steepening in the intermediate region. Both the flattening and the steepening are more marked at higher N_{Pr} and N_{Sc}. All of the trends cited in connection with Figures 7 and 8 are consistent with the Nusselt and Sherwood number results.

PHASE CHANGE AT ONE WALL AND PRESCRIBED PLENUM CONDITIONS AT THE OTHER WALL

Attention is now turned to generalizing the foregoing analysis and results. Consideration is given to a channel wherein wall 1 is coated with an evaporable (or sublimable) material, while a binary gas mixture, one of whose constituents is the evaporable vapor, is injected through wall 2. Neither the temperature, the mass fraction, nor the mass transfer rate is specified at the evaporating surface; rather, these quantities are determined by the dynamics of the problem and from saturation state information. With respect to the injected gas, its temperature and mass fraction are specified in the plenum chamber located behind wall 2. The temperature and mass fraction at the surface of wall 2 are also determined by the dynamics of the problem.

Generalizing Analysis

The essential ingredients of the generalizing analysis are mass and energy balances at the channel walls. The derivation of the balance equations for wall 2 is facilitated by reference to Figure 1*b*, which shows a control volume

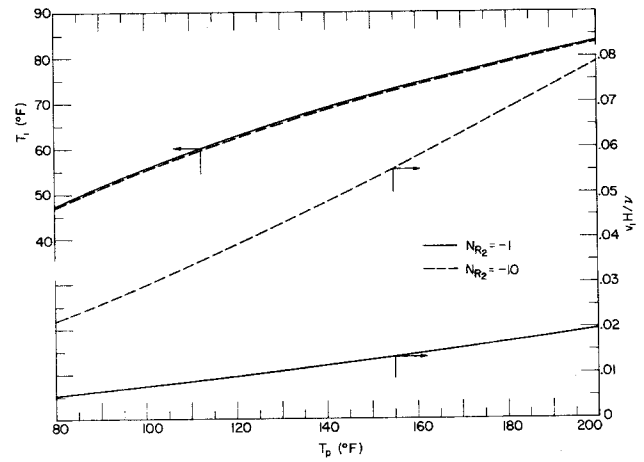

Fig. 9. Temperature and evaporation rate of a layer of liquid water.

spanning the wall and extending into the plenum chamber. Mass conservation requires that inflow and outflow be in balance for each of the component species or, equivalently, for one of the components and for the mixture as a whole. If $\dot{m}$ denotes the mass rate of mixture flow per unit area and $\dot{m}_i$ denotes the mass rate of flow of component i, then

$$\dot{m}_2 = \dot{m}_p, \quad \dot{m}_{i2} = \dot{m}_{ip} \tag{27}$$

In the plenum, mass diffusion is negligible, so that

$$\dot{m}_{ip} = W_{ip}\ \dot{m}_p \tag{28a}$$

However, at station 2, both convection and diffusion contribute, with the result that

$$\dot{m}_{i2} = \rho_{i2} v_2 - \rho_2 D\ (\partial W_i/\partial y)_{y=H} \tag{28b}$$

and, furthermore, since $\partial W_i/\partial y + \partial W_j/\partial y = 0$

$$\dot{m}_2 = \rho_2 v_2 \tag{28c}$$

By bringing together Equations (27), (28*a*), (28*b*), and (28*c*), and by introducing the Sherwood number from Equation (25), there follows

$$W_{i2} = \frac{W_{ip} - W_{i1}\ (N_{Sh_2}/N_{R_2}\ N_{Sc})}{1 - (N_{Sh_2}/N_{R_2}\ N_{Sc})} \tag{29}$$

which relates the unknown W_{i2} with other parameters of the problem and thereby facilitates its subsequent elimination.

Next, an energy balance is made for the control volume of Figure 1*b*. Upon noting that $\dot{m}_2 = \dot{m}_p = \rho_2 v_2$, the balance can be written as

$$\rho v_2 c_p (T_p - T_2) = -k(\partial T/\partial y)_{y=H} \tag{30}$$

After rearrangement and introduction of the Nusselt number from Equation (24), the foregoing becomes

$$T_2 = \frac{T_p - T_1\ (N_{Nu_2}/N_{R_2}\ N_{Pr})}{1 - (N_{Nu_2}/N_{R_2}\ N_{Pr})} \tag{31}$$

which will be employed later to eliminate the unknown T_2.

Now, turning to wall 1, suppose that species i represents the vapor of the material that is evaporating or subliming. Then, in general, the surface of wall 1 will be impermeable to species j; that is, $\dot{m}_{j1} = 0$, or

$$\rho_{j1} v_1 = \rho_1 D\ (\partial W_j/\partial y)_{y=0} \tag{32}$$

which becomes, after substitution of dimensionless variables and by using the relations $\partial W_j/\partial y = -\partial W_i/\partial y$ and $W_j = 1 - W_i$

$$\frac{W_{i2} - W_{i1}}{1 - W_{i1}}\ (N_{Sh_1}/N_{R_2}\ N_{Sc}) = \beta \tag{33}$$

Furthermore, if wall 1 is insulated from the external environment, the latent heat requirements of the phase change process must be fulfilled by convective heat transfer from the channel flow to the wall. In mathematical terms, such an energy balance takes the form

$$k(\partial T/\partial y)_{y=0} = \rho_1 v_1 \lambda \tag{34}$$

The dimensionless form of Equation (34) is

$$\frac{c_p(T_1 - T_2)}{\lambda}\ (N_{Nu_1}/N_{R_2}\ N_{Pr}) = \beta \tag{35}$$

The derivations of the foregoing paragraphs have yielded four balance Equations, (29), (31), (33), and (35), respectively. Among these, the unknowns W_{i2} and T_2 may be eliminated, leaving

$$\frac{W_{ip} - W_{i1}}{1 - W_{i1}}\ \frac{(N_{Sh_1}/N_{R_2}\ N_{Sc})}{1 - (N_{Sh_2}/N_{R_2}\ N_{Sc})} = \beta \tag{36}$$

and

$$\frac{c_p(T_1 - T_p)}{\lambda}\ \frac{(N_{Nu_1}/N_{R_2}\ N_{Pr})}{1 - (N_{Nu_2}/N_{R_2}\ N_{Pr})} = \beta \tag{37}$$

Equations (36) and (37), taken together with the relations $N_{Nu} = N_{Nu}\ (N_{R_2}, \beta, N_{Pr})$, $N_{Sh} = N_{Sh}\ (N_{R_2}, \beta, N_{Sc})$, and with the saturation state information, provide a means for determining the unknowns T_1, W_{i1}, and β for given values of T_p, W_{ip}, and N_{R_2}. The first step in the calculation method is to select a trial value of β. This, together with the specified N_{R_2} and the known N_{Sc}, gives N_{Sh_1} and N_{Sh_2} (that is, from the appropriate among Figures 3 through 6). Then, from Equation (36), W_{i1} is calculable and, in turn, T_1 follows by employing saturation state information.

Next, with the trial value of β, the specified N_{R_2} and the known N_{Pr}, N_{Nu_1} and N_{Nu_2} are found. This information is used to evaluate T_1 from Equation (37). The T_1 values, respectively, given by Equations (36) and (37) are compared. If these are identical, then the trial value of β is acceptable. If not, a new β value is selected, and the procedure is repeated.

Once $\beta\ (= -v_1/v_2)$ is determined, then the evaporation (or sublimation) rate is also determined, since v_2 is known from the specified value of N_{R_2}.

To illustrate the just described calculation procedure, results for the temperature T_1 and the evaporation rate $\rho_1 v_1$ were determined for the situation in which a layer of liquid water covers wall 1 and hot air is injected through wall 2. This problem was worked out with the drying of sheetlike materials in mind, for instance, photographic film and paper. Such a sheet, corresponding to wall 1 in Figure 1, may move slowly in the direction normal to the x, y plane. In practice, wall 2 is a perforated plate through which a hot gas is injected.

The calculations were performed for the case in which the gas in the plenum behind wall 2 is pure air, with plenum temperatures T_p ranging from 80° to 200°F. N_{R_2} was assigned values of -1 and -10, and the static pressure level in the channel was 1 atm. In executing the calculations, Figures 3 and 4 were, respectively, employed for the Sherwood and Nusselt numbers.

Numerical results corresponding to the just described conditions are presented in Figure 9. The figure shows that, as expected, the evaporation rate increases as the temperature level of the incoming air stream is raised. The evaporation rate also increases as the injection rate of the air increases, but the augmentation of the evaporation rate

is substantially smaller than is the causative increase in the airflow rate. The surface temperature of the water is raised as the air temperature rises. Over the span of plenum temperatures T_p from 80° to 200°F., T_1 varies from about 47° to 83°F., essentially independent of N_{R2}.

ACKNOWLEDGMENT

The authors gratefully acknowledge the assistance of Yung-cheng Yu in various aspects of the numerical computations.

NOTATION

D = mass diffusion coefficient
D_e = equivalent diameter, $2H$
f = velocity function, Equation (6)
H = channel height
h = heat transfer coefficient, Equation (24)
K = mass transfer coefficient, Equation (25)
k = thermal conductivity
$\dot{m}$ = mass flow/time area
N_{Nu} = Nusselt number, hD_e/k
N_{Pr} = Prandtl number, ν/α
N_{R_2} = injection Reynolds number, v_2H/ν
$N_{R\bar{u}}$ = axial Reynolds number, $\bar{u}H/\nu$
N_{Sc} = Schmidt number, ν/D
N_{Sh} = Sherwood number, $KH/\rho D$
p = pressure
T = temperature
u = axial velocity
$\bar{u}$ = mean velocity
v = transverse velocity
W = mass fraction
x = axial coordinate
y = transverse coordinate

Greek Letters

α = thermal diffusivity
β = injection ratio, $-(v_1/v_2)$
η = dimensionless coordinate, y/H
λ = latent heat
ν = kinematic viscosity
ρ = density
Φ_T = temperature variable, $(T - T_1)/(T_2 - T_1)$
Φ_W = mass fraction variable, $(W_i - W_{i1})/(W_{i2} - W_{i1})$
Ω_T = Prandtl number
Ω_W = Schmidt number

Subscripts

i, j = mixture components
p = plenum chamber
1 = wall with lesser $|v|$
2 = wall with greater $|v|$

LITERATURE CITED

1. Berman, A. S., *J. Appl. Phys.*, **24**, 1232 (1953).
2. Terrill, R. M., and G. M. Shrestha, *ZAMP*, **16**, 470 (1965).
3. Terrill, R. M., *Intern. J. Heat Mass Transfer*, **8**, 1491 (1965).
4. Gill, W. N., Eduardo del Casal, and D. W. Zeh, *AIChE J.*, **12**, 266 (1966).
5. Huesmann, K., and E. R. G. Eckert, "Untersuchungen über die laminare Strömung und dem Umschlag zur Turbulenz in Porösen Rohren mit gleichmässiger Einblasung durch die Rohrwand," Vol. 1, p. 1, *Wärme- und Stoffübertragung*, Germany (1968).
6. Rodi, W., *Heat Transfer Lab. Rept. No. 79*, Univ. Minn., Minneapolis (Feb., 1968).
7. Sherwood, T. K., and R. L. Pigford, "Absorption and Extraction," McGraw-Hill, New York (1952).

Manuscript received November 4, 1968; revision received January 10, 1969; paper accepted January 14, 1969.

Initiation of Thermal Convection in Finite Right Circular Cylinders

IVAN CATTON and D. K. EDWARDS

University of California, Los Angeles, California

Linear perturbation analyses are extended to determine the lowest Rayleigh number at which convection initiates in a vertical cylinder heated on the bottom and cooled on the top. The critical Rayleigh number for the first mode of convection in a right circular cylinder with a perfectly conducting wall is shown to be three times larger than that in such a cell with a perfectly adiabatic side wall. An adjusted wave number is shown to make the results of Pellew and Southwell applicable to the adiabatic wall in a manner similar to that used by Pnueli and Ostrach for the perfectly conducting side wall. The results are compared with experiment and are in very good agreement.

It has long been known that a thermally expansive fluid enclosed between horizontal plates and heated from below starts to convect only when a critical temperature gradient is surpassed. After Benard's (*1*) observations, Rayleigh (2) gave a theoretical explanation of such a phenomenon, neglecting effects of surface tension and shear stress on the horizontal boundaries. Pellew and Southwell (3) found an exact solution to the linearized perturbation equations, taking account of shear at the horizontal boundaries.

Malkus (*4*) pointed out that not only is there a first critical Rayleigh number (as the critical dimensionless